Fractal dimension and unscreened angles measured for radial viscous fingering

Olivier Praud and Harry L. Swinney
Center for Nonlinear Dynamics and Department of Physics, The University of Texas at Austin, Austin, Texas 78712, USA
(Received 15 November 2004; published 21 July 2005)

We have examined fractal patterns formed by the injection of air into oil in a thin (0.127 mm) layer contained between two cylindrical glass plates of 288 mm diameter (a Hele-Shaw cell), for pressure differences in the range $0.25 \leqslant \Delta P \leqslant 1.75$ atm. We find that an asymptotic structure is reached at large values of the ratio r/b, where r is the pattern radius and b the gap between the plates. Both the driving force and the size of the pattern, which reaches $r/b=900$, are far larger than in past experiments. The fractal dimension D_0 of the pattern for large r/b is 1.70 ± 0.02. Further, the generalized dimensions D_q of the pattern are independent of q, $D_q \simeq 1.70$ for the range examined, $-11 < q < 17$; thus the pattern is self-similar within the experimental uncertainty. The results for D_q agree well with recent calculations for diffusion-limited aggregation (DLA) clusters. We have also measured the probability distribution of unscreened angles. At late times, the distribution approaches a universal (i.e., forcing and size-independent) asymptotic form that has mean 145° and standard deviation 36°. These results indicate that the distribution function for the unscreened angle is an invariant property of the growth process.

DOI: 10.1103/PhysRevE.72.011406 PACS number(s): 61.43.Hv, 68.03.Kn, 47.20.Hw

I. INTRODUCTION

Highly branched fractal structures develop in a variety of problems including directional solidification, crystallization, dendritic growth, chemical electrodeposition, growth of bacterial colonies, combustion fronts, and viscous fingering [1–4]. Viscous fingers grow when a low viscosity fluid displaces a high viscosity fluid. We consider here viscous fingering patterns formed between two closely spaced radial plates (a Hele-Shaw cell) where the less viscous fluid is injected in the center and a fractal pattern then grows outward. In the radial geometry, the growing fingers continually split because of the interfacial instability, thus generating new fingers and side branches.

In order to obtain a complex pattern with a wide range of scales, the characteristic length scale of instability of the interface must be as small as possible. This instability length, sometimes called the capillary length, is

$$\lambda_c = \pi b \sqrt{\frac{\sigma}{\mu V}}, \tag{1}$$

which corresponds to the most unstable wavelength given by a linear stability analysis of a planar interface between a less viscous fluid and a more viscous fluid [5]. Here V is the velocity of the interface, b is the gap thickness of the cell, σ is the interfacial tension, and μ is the difference between the viscosities of the two fluids, where the less viscous fluid is forced in the direction of the more viscous fluid. Thus small λ_c is achieved by having b and σ small and μ and V large. Our cell is especially designed to achieve small λ_c.

Paterson [6] pointed out that the growth of viscous fingering patterns, an archetype of growth in a Laplacian field, is similar to the growth of aggregates produced by the numerical model of diffusion limited aggregation (DLA) introduced by Witten and Sander [7]. In both systems, a highly ramified pattern develops with most of the growth occurring at the extremities, while the inner region is screened and remains unmodified during further pattern development. However, the relation between the Laplacian growth problem and the continuum limit of DLA remains an open question that is still debated [8–11].

The statistical and geometrical properties of radial viscous fingering patterns have been examined in a few previous experiments. Measurements of the fractal dimension D_0 of the patterns [12–14] yielded results slightly higher but consistent with the dimension of DLA clusters. However, the range of length scales where scaling held was small, and very few studies examined the spectrum of generalized dimensions, D_q. Couder [13] found that for $q \geqslant 0$, the values of D_q were nearly constant and close to the values observed for DLA aggregates.

In this paper, we present measurements of the spectrum of generalized dimensions for viscous fingering patterns formed in a radial Hele-Shaw cell for driving forces and pattern size much larger than previous experiments. Our goal is to understand the geometrical and growth properties of the patterns at asymptotically long times and high forcing, where the Laplacian growth is conjectured to reach a universal form.

We note that our measurements concern the viscous fingering pattern itself, not its harmonic measure, which is the probability measure of the pressure gradient field surrounding the pattern. Many studies of DLA have concerned the fractal geometry of the harmonic measure rather than that of the DLA cluster. (For DLA, the harmonic measure is the probability measure for a random walker coming from infinity to hit the boundary of a cluster.) DLA clusters are self-similar, that is, D_q has the same value for all q [15], while the harmonic measure is a multifractal [15–17] with D_q depending on q.

Fractal dimensions D_q provide information about geometrical properties that can be compared for various branched fractal patterns and models. However, additional information is needed to describe the growth process, which has not yet received a general theoretical treatment. The possible existence of a critical screening angle in Laplacian

growth has recently received much attention, as it could provide a clue to a hierarchical fractal ordering [18–24]. Pattern growth occurs primarily at the outer edges of the pattern; the region to either side of a fast growing tip is screened. Studies of a "threshold screening model," which has a screening parameter that can be varied, have yielded a critical value of a screening constraint, $\Theta_c \approx 130°$, where the patterns changed from compact to one-dimensional [23,25] and the radial symmetry was broken. Although the model's screening constraint is not a parameter that can varied in experiments, some indication of the possible existence of a critical angle was obtained by Lajeunesse and Couder [18], who studied growth in wedges. They observed that for a wedge angle $\Theta > \Theta_c = 90°$, two main branches coexisted, while for smaller angles the instability failed to create two independent long-lived structures—one branch stopped growing. They argued that the critical angle they determined was probably underestimated, the pattern being too small to have reached an asymptotic state.

Screening of the growth of DLA patterns was studied by Arneodo and co-workers [19–21], who used the "wavelet transform microscope" to investigate the distribution of branching angles of a cluster at different scales. They suggested the existence of a fivefold symmetry associated with a critical angle $\Theta_c = 144°$. Screening for DLA patterns grown in the wedge geometry was examined by Kessler *et al.* [22], who found a critical wedge angle $120° < \Theta_c < 140°$, below which only one main branch existed. Screening was also examined in experiments on electroless deposits in the diffusion-limited regime by Kuhn *et al.* [24], who measured the angle between branches at different scales and found a predominance of fivefold symmetry.

However, the screening effect has not been examined in experiments on viscous fingering patterns in the axisymmetric configuration. We report here measurements and analysis of the distribution of *unscreened* angles. Our measurements reveal a self-similar probability distribution of the unscreened angles once the asymptotic stage of the growth is reached.

In the following section we describe our experimental system and present images of growing viscous fingering patterns. Results for the fractal dimension D_0 and the generalized dimensions D_q are presented in Secs. III and IV, respectively. Measurements of the probability distribution for the unscreened angles are presented in Sec. V, and the conclusions are given in Sec. VI.

II. EXPERIMENTAL SETUP AND DESCRIPTION OF THE GROWTH

A. System

The system we have used to generate radial viscous fingering patterns is shown schematically in Fig. 1. The cell is the same as the one used by Sharon *et al.* [26]. It consists of two 288 mm diameter optically polished circular glass plates (60 mm thick), which are flat to 0.13 μm and separated by a gap b of 0.127 mm. The plates are clamped into an aluminum holder with a 25.4 mm thick Plexiglas clamp, which seals a 12.7 mm annular buffer around the plates. The buffer and gap are filled with a silicone oil (viscosity $\mu = 345$ mPa s, surface tension $\sigma = 21.0$ mN/m).

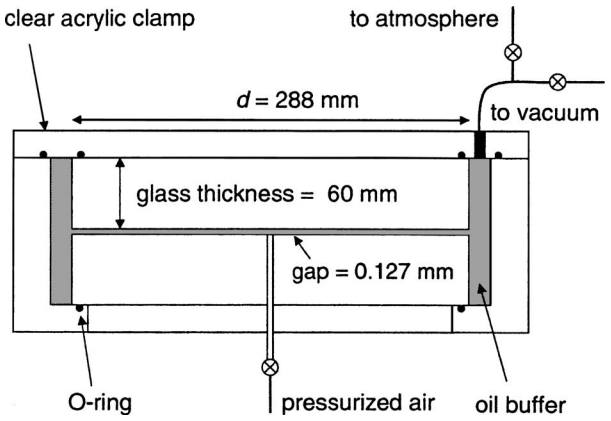

FIG. 1. A cross section of the radial Hele-Shaw cell. The pressure of the air injected through the center hole was adjusted from 1 to 1.75 atm, while the pressure in the oil buffer was set to 10^{-3} or 1 atm. The thick optically polished plates provide a gap that is uniform to better than 2% even at the highest pressure difference.

Patterns are formed by imposing a constant air pressure P_{in} at a hole in the center of the bottom plate, while the pressure P_{out} for the oil buffer around the cell (see Fig. 1) is set to either 10^{-3} atm or to 1 atm. The high rigidity and flatness of the plates permit us to achieve large pressure differences while keeping the variation in the gap very small. This system provides a well-defined pressure difference, ΔP, which had four values in the experiments presented here: 0.25, 0.50, 1.25, and 1.75 atm. With this forcing system, the finger velocity is essentially constant during the growth process, as can be seen in Fig. 2(a). The lengths λ_c and the nondimensional Capillary numbers Ca (where $\mathrm{Ca} = \mu V/\sigma$) obtained for the finger velocities illustrated in Fig. 2(b) for $\Delta P = 0.25$, 0.50, 1.25, and 1.75 atm are, respectively, $(\lambda_c, \mathrm{Ca}) = (1.18\ \mathrm{mm}, 0.12)$, $(0.79\ \mathrm{mm}, 0.26)$, $(0.49\ \mathrm{mm}, 0.66)$, and $(0.41\ \mathrm{mm}, 0.96)$. The smallest λ_c is about three times the gap thickness b.

The view through the upper plate is unobstructed; hence the entire viscous fingering structure can be observed at all times. Using a digital camera (DVC-1300, 1300×1030 pixels) at 12 frames/s, we obtain images throughout the entire growth process with a spatial resolution of $2b$. Subtraction of background and thresholding then provide binary images of the two phases; these are used to determine the geometrical properties of the interface.

B. Growth of a pattern

The initial growth generates a circular front that becomes unstable and develops protrusions that grow and evolve, as illustrated by the time sequence in Fig. 3. Growth of a viscous fingering structure is compared to that of a DLA cluster [27] in Fig. 4. Fast growing protrusions of the viscous fingering pattern screen the slow growing protrusions, which slow and ultimately stop. Simultaneously, the fastest growing tips have more space to grow, and they become unstable to tip-splitting, continually generating smaller scales. In the ra-

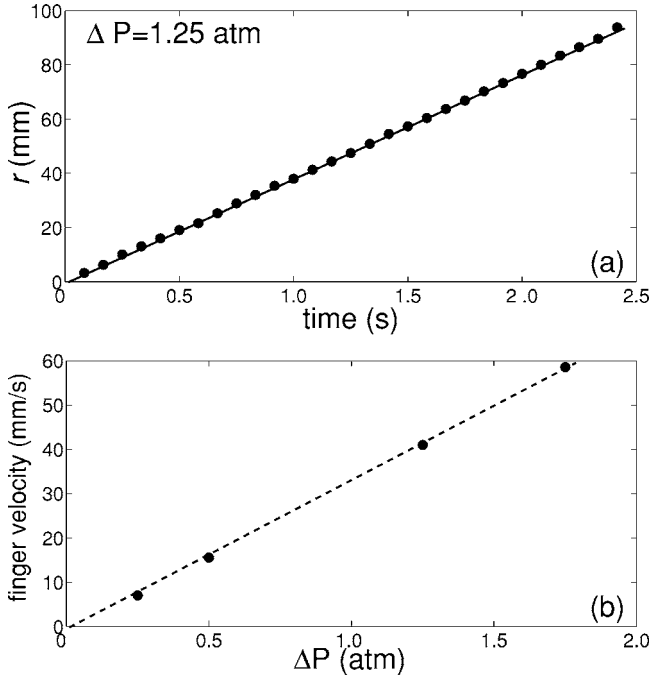

FIG. 2. (a) The distance r from the center of the pattern to the most distant finger tip for a pressure difference $\Delta P=1.25$ atm. The velocity is essentially constant; hence the instability length λ_c is constant throughout the growth process, except for a very small but discernible increase when the finger tip begins to feel the outer boundary. (b) The velocity of the finger tip increases linearly with the pressure drop ΔP.

dial geometry there is no large length scale such as the channel width in the channel geometry, and a steady state cannot be achieved. The growing pattern becomes more and more complex and highly ramified. At high pressures, the resultant highly branched patterns have a minimum finger width more than two orders of magnitude smaller than the pattern size (see Fig. 3, $t=2.8$ s).

III. FRACTAL DIMENSION D_0

The determination of the fractal or box dimension D_0 of the asymptotic pattern (e.g., Fig. 3, $t=2.8$ s) is illustrated in Fig. 5. The data for each value of $\Delta P=0.25$, 0.50, 1.25, and 1.75 atm were obtained, respectively, from 9, 12, 12, and 4 experimental realizations of asymptotic patterns ($r/b>800$). The fractal dimension was obtained from the slope of $\log N(\epsilon)$ versus $\log \epsilon$ for small ϵ, where $N(\epsilon)$ is the number of boxes of size ϵ needed to cover the pattern. The local slope is shown as a function of ϵ in Fig. 5(b).

The slope is essentially independent of ΔP and ϵ for $0.6<\log_{10}(\epsilon)<1.7$; this slope yields $D_0=1.70\pm0.02$. The scaling is cut off at small scales by the effect of surface tension, which inhibits the formation of branches with scales smaller than λ_c; also, at small scales, ϵ becomes comparable to b and the third dimension can no longer be ignored. For large values of ϵ, the pattern size approaches the container size, and finite-size effects become important.

We made two tests to gain confidence in our dimension algorithm: (i) D_0 was computed using the correlation function algorithm [28,29], and (ii) our box counting algorithm was applied to fractals of known dimension. For the first test we computed the density-density correlation function $C(r)=\langle\rho(r')\rho(r'+r)\rangle$ (normalized at $r=0$) with $\rho=1$ in the air phase and $\rho=0$ in the oil phase; the average was performed over 12 realizations. As illustrated in Fig. 6, at intermediate length scales $C(r)$ decays as a power law $r^{-\delta}$; the decay exponent is related to the fractal dimension of the pattern by $D_0=2-\delta$ [26]. We obtain $C(r)\propto r^{-0.29\pm0.03}$ over nearly a decade of r, which yields $D_0=1.71\pm0.03$, consistent with the result from the box counting algorithm.

We tested the box counting algorithm directly by examining several fractals of known dimension, such as the Sierpinski Carpet and the Sierpinski Gasket [30]. These fractals were generated with the same experimental resolution as the experimental data. For example, the Sierpinski Gasket in Fig. 7(a) has a size 751×751 pixels (six iterations). The resultant scaling range was about one decade, as Fig. 7(b) shows. The values deduced for D_0 for this fractal and for others with known dimension were always within 1% of the correct values. Box counting algorithms have been shown to slightly underestimate dimension values [31,32], and that was the case for the fractals of known dimension that we examined (e.g., Fig. 7).

Table I compares our result for D_0 with results from previous experiments on radial viscous fingering and with calculations of D_0 for DLA clusters. Our value of D_0 for radial viscous fingering patterns is consistent with but slightly smaller than the values obtained by Rauseo *et al.* [12], Couder [13], and May and Maher [14]. However, we have

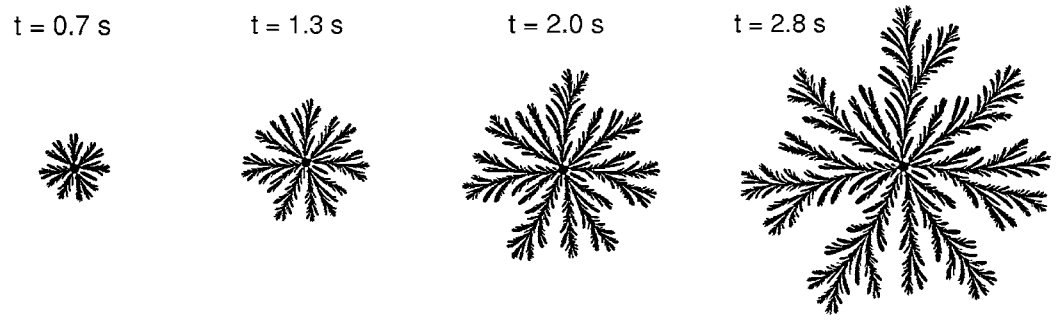

FIG. 3. Snapshots of the radial pattern at different times during the growth for $\Delta P=1.25$ atm. At $t=2.8$ s, the radius of the pattern is 113 mm ($r/b=890$).

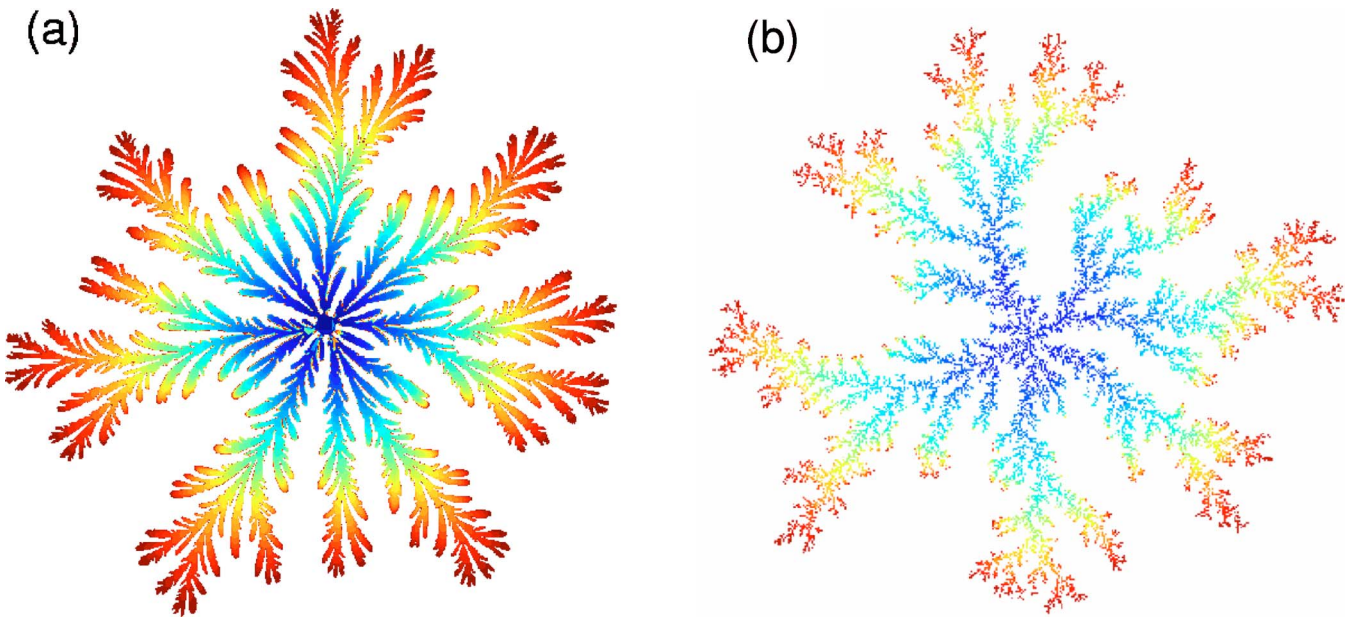

FIG. 4. (Color online) Comparison of the time evolution of the radial growth patterns for (a) viscous fingering ($\Delta P = 1.25$ atm) and (b) diffusion limited aggregation [27]. The colors indicate the ages of the patterns; the oldest (first created) region is blue and the youngest is red.

achieved an order of magnitude larger forcing, as indicated in Table I by values of the dimensionless forcing parameter

$$C = Q\mu/b\sigma, \tag{2}$$

where Q is the areal rate of injection of air. We use the parameter C [not to be confused with the correlation function $C(r)$] because its value was given in earlier papers. In our case, Q is not a constant but is estimated by measuring the instantaneous increase in size of the pattern at $r/b \sim 800$. Although a previous experiment [12,14] also used thick glass plates to keep plate flexing to a minimum, that experiment did not achieve conditions of such high forcing with a well-defined, constant, and homogeneous plate separation; the upward pressure on the top plate lifted it and limited the forcing range. Our use of firmly clamped optically polished (to 0.2 micrometer rms flatness) plates of 60 mm thickness provides a well-defined plate separation (see Sec. II). Also our fractals are larger than in previous experiments—see in Table I the values of r_{max}/b, where r_{max} is the radius of the largest growth.

In Sec. V we show that, for the range of forcing studied, the distribution function for the unscreened angle approaches its asymptotic form at $r/b \approx 500$. The large values of C and r/b achieved in our experiments were not accessible in previous experiments (see Table I), but appear to be essential for determining asymptotic properties of a developing viscous fingering pattern (see Sec. V). Thus we conclude that 1.70 ± 0.02 is the asymptotic value for the fractal dimension.

The independence of D_0 on the forcing observed here confirms and extends to a higher value of the driving force the results of Rauseo *et al.* [12] and May and Maher [14]. Rauseo *et al.* [12] observed no discernible dependence of D_0 with the forcing in the range they investigated ($1.1 < C < 35$). May and Maher [14] found that the fractal dimension was approximatively 1.71 for $10 < C < 40$ and suddenly increased to an apparent asymptotic value of 1.79 as the driving force became large ($C \geqslant 40$); it did not change with further increase of the forcing. A different result was obtained in earlier experiments by Ben-Jacob *et al.* [33], who found that the fingering pattern went over to a "dense-branching" morphology with a fractal dimension of 2 as an asymptotic late stage of development was approached. Couder [13] and May and Maher [14] pointed out that the Ben-Jacob *et al.* result may have been a consequence of the flexing of the Plexiglas plates used in their experiments.

Some experiments have used a constant areal injection rate Q [12,14], which means that the finger tip velocity decreases as the flow progresses, leading to λ_c increasing with time (1). This leads to an overestimate of the fractal dimensional. Also, conditions in which the smallest scale (λ_c) increases with growth are not appropriate for comparisons with DLA, since the smallest length scale for a DLA cluster (the size of a random walker) is fixed. Therefore, rather than use constant Q, we follow Couder [13] and use a constant pressure difference, which produces a constant λ_c for a growing cluster.

Our result for D_0 is consistent with the most recent numerical estimates of the fractal dimension of DLA aggregates, $D_0 = 1.713 \pm 0.003$ [34–36] (see Table I). This result suggests a similar fractal morphology of the two growth phenomena but contrasts sharply with Barra *et al.*'s prediction that the asymptotic fractal dimension of Laplacian growth patterns should be higher than the fractal dimension of DLA and bounded from below by 1.85 and could possibly be as high as 2 [9,11].

IV. GENERALIZED FRACTAL DIMENSIONS

Further characterization of the viscous fingering patterns can be achieved by determining the generalized or Renyi

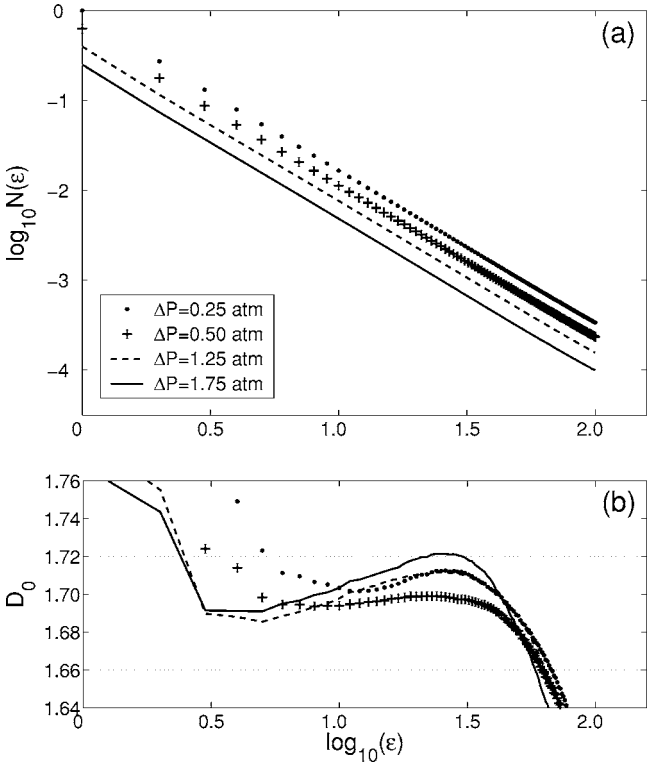

FIG. 5. Determination of the fractal dimension D_0 for the viscous fingering patterns for the different forcing conditions, $\Delta P = 0.25$, 0.50, 1.25, and 1.75 atm. The fractal dimension is computed for the asymptotic pattern ($r/b > 800$). (a) The value of D_0 is given by the slopes of the graphs of $\log_{10}N(\epsilon)$ as a function of $\log_{10}(\epsilon)$, where N has been normalized by the number of boxes of size one pixel needed to cover the pattern. Curves for successively larger values of ΔP are shifted downward by −0.2 to facilitate comparison. (b) Values of D_0 given by the local slopes computed from a linear least squares fit over the interval $\Delta \log_{10}(\epsilon) = 0.45$. These values are nearly independent of ΔP and are approximately constant in the range $0.6 < \log_{10}(\epsilon) < 1.7$. From these measurements we conclude $D_0 = 1.70 \pm 0.02$ in the range studied.

dimensions D_q, which are defined for all real values of the index q [37]. The dimension D_q is a generalization of the box counting definition: cover the pattern with a grid of square boxes of size ϵ and define $p_i(\epsilon)$ to be the relative portion of the pattern in cell i, and define $N(\epsilon)$ to be the total number of boxes of size ϵ needed to cover the whole pattern. Then D_q is given by [31,38]

$$D_q = \lim_{\epsilon \to 0} \frac{1}{q-1} \frac{\log Z_q(\epsilon)}{\log \epsilon}, \tag{3}$$

where Z_q is the partition function,

$$Z_q(\epsilon) = \sum_{i=1}^{N(\epsilon)} p_i(\epsilon)^q. \tag{4}$$

Thus the index q corresponds to the order of the moments of p_i at length scale ϵ.

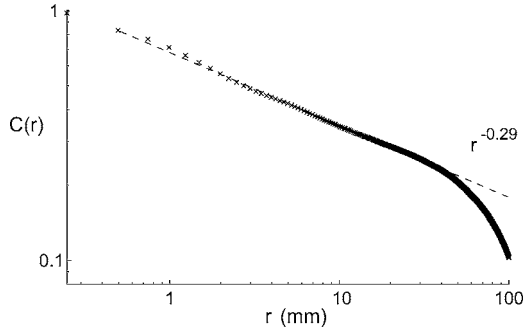

FIG. 6. Average density-density correlation function, $C(r)$. The dashed line shows a fit to the fractal scaling region where $C(r) \sim r^{0.29 \pm 0.03}$, yielding a fractal dimension of $D_0 = 1.71 \pm 0.03$. From [26].

The limit of Eq. (3) is not experimentally accessible, but D_q can be obtained from the slope of graphs of $\log Z_q/(q-1)$ as a function of $\log(\epsilon)$. We determine D_q by averaging Z_q over 50 randomly located grids for each size ϵ. In addition, Z_q values are averaged over all the realizations for a given experimental condition. Results for D_q for $q \geqslant 0$ are shown in Fig. 8(a). As in the determination of D_0, there is a limited range where scaling is observed and in which the

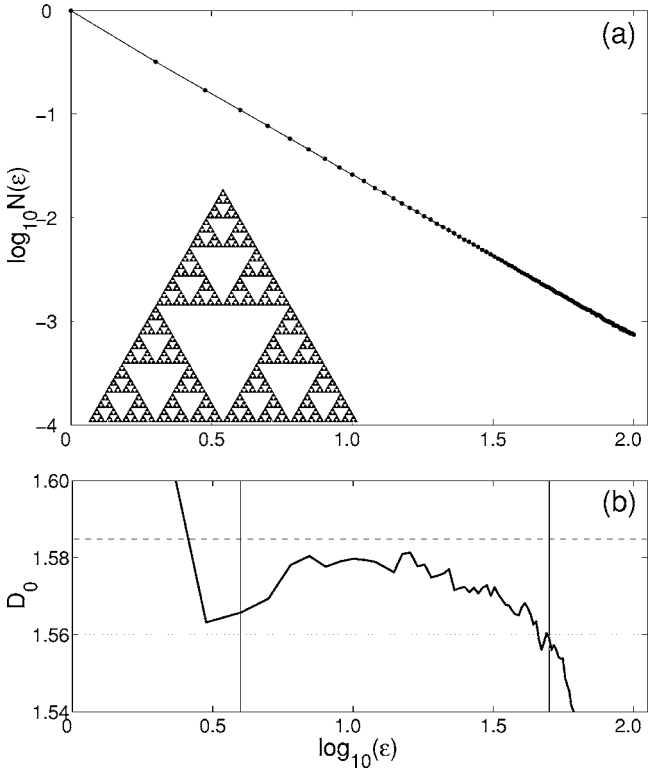

FIG. 7. These graphs illustrate the determination of D_0 for a fractal of known dimension, the Sierpinski gasket [30], which is shown in the inset of (a). The plot in (a) of $\log_{10}N(\epsilon)$ vs $\log_{10}(\epsilon)$ was used to obtain D_0 from the local slope computed over the interval $\Delta \log_{10}(\epsilon) = 0.45$. The result for the entire scaling range $0.6 < \log_{10}(\epsilon) < 1.7$ is $D_0 = 1.575 + 0.020$, which is just 0.6% smaller than the known value, $(\log 3)/(\log 2) = 1.584\,96$, indicated by the horizontal dashed line.

TABLE I. Values of the fractal dimension D_0 obtained for viscous fingering patterns and diffusion limited aggregation patterns. C_{max} is the maximum value of the forcing parameter C, which is defined in Eq. (2).

Authors	D_0	Comment	C_{max}	r_{max}/b
Praud and Swinney	1.70±0.02	radial viscous fingering	800	900
Rauseo *et al.* [12]	1.79±0.07	radial viscous fingering	35	190
Couder [13]	1.76	radial viscous fingering		
May and Maher [14]	1.79±0.04	radial viscous fingering	75	190
Witten and Sander [7]	1.70±0.02	square lattice radial DLA		
Tolman and Meakin [34]	1.715±0.004	off-lattice radial DLA		
Ossadnik [35]	1.712±0.003	off-lattice radial DLA		
Davidovitch *et al.* [36]	1.713±0.003	DLA (conformal map theory)		

pattern can be considered as a fractal object: the local slopes depend only very weakly on q and ϵ for $1.1 \leqslant \log_{10}(\epsilon) \leqslant 1.8$, and yield $D_q = 1.70 \pm 0.04$ for $0 \leqslant q \leqslant 17$. This result supports earlier measurements that suggested D_q is nearly constant and equal to D_0 for viscous fingering patterns [13].

The fixed-sized algorithm is suitable for $q \geqslant 0$ but not for $q < 0$ because it is difficult to determine small values of p_i accurately. Therefore, for $q < 0$ we use a fixed-mass algorithm introduced by Badii and Politi [39]. In this method, D_q is obtained from

$$\frac{\tau}{D_q} = \lim_{m \to 0} \frac{\log\langle [\epsilon(m)]^{-\tau} \rangle}{\log m}, \tag{5}$$

where $\epsilon(m)$ is the size of a box, centered at random on the pattern and containing a relative portion m of the pattern. We implement Eq. (5) as follows: we choose a random location in the pattern and then increase the box size ϵ, evaluating at each growth step the measure m contained in such a box. Repeating this procedure over 1000 randomly located points gives pairs of values (ϵ, m). With this set we can evaluate the average, $\langle [\epsilon(m)]^{-\tau} \rangle$, for each discretized measure m. We then average over all the realizations. The value of D_q can then be extracted from the slope of a graph of $\log\langle [\epsilon(m)]^{-\tau} \rangle$ as a function of $\log(m)$. Figure 8(b) illustrates the determination of D_q for $q < 0$, using the fixed-mass algorithm. The values of D_q show only a weak dependence on q and m in a range of the measure m that extends from $\log_{10}(m) = 2.2$ to $\log_{10}(m) = 3.9$. We conclude that, for $-11 < q < -0.2$, $D_q = 1.7 \pm 0.1$, in agreement with D_0 and with D_q for $q > 0$. The scatter in the

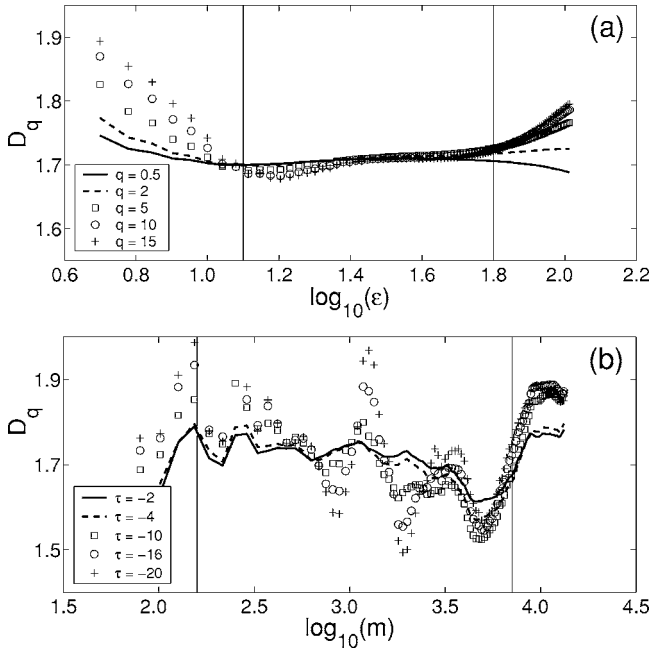

FIG. 8. These graphs illustrate the determination of the generalized fractal dimensions D_q for a particular experimental condition, $\Delta P = 1.25$ atm. (a) Value of D_q for $q > 0$, obtained from the local slopes of graphs of $(\log Z_q)/(q-1)$ versus $\log(\epsilon)$. D_q is constant and independent of q for nearly a decade of length scale. The D_q values obtained from the data between the vertical lines are shown in Fig. 9. (b) Value of D_q for $q < 0$, obtained from the local slopes of the graphs $\log\langle [\epsilon(m)]^{-\tau} \rangle$ as a function of $\log(m)$ (fixed-mass algorithm). The average values of q for the values of τ in the graph are $(\tau, q) = (-2, -0.2)$, $(-4, -1.3)$, $(-10, -4.9)$, $(-16, -8.5)$, and $(-20, -10.8)$.

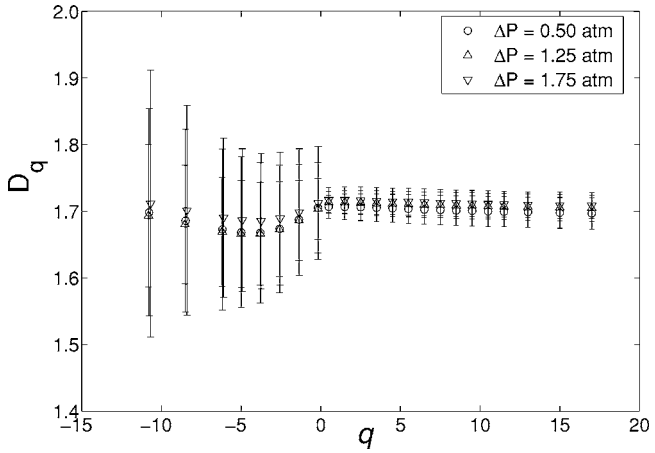

FIG. 9. Results from fixed-size ($q \geqslant 0$) and fixed-mass ($q < 0$) computations of the generalized fractal dimension D_q. The measurements indicate no dependence of D_q on ΔP. The data yield $D_0 = 1.70 \pm 0.02$, $D_q = 1.70 \pm 0.04$ for $0 \leqslant q \leqslant 17$, and $D_q = 1.7 \pm 0.1$ for $-11 \leqslant q < 0$. Hence the fractal viscous fingering patterns are self-similar objects with a fractal dimension 1.70, independent of q.

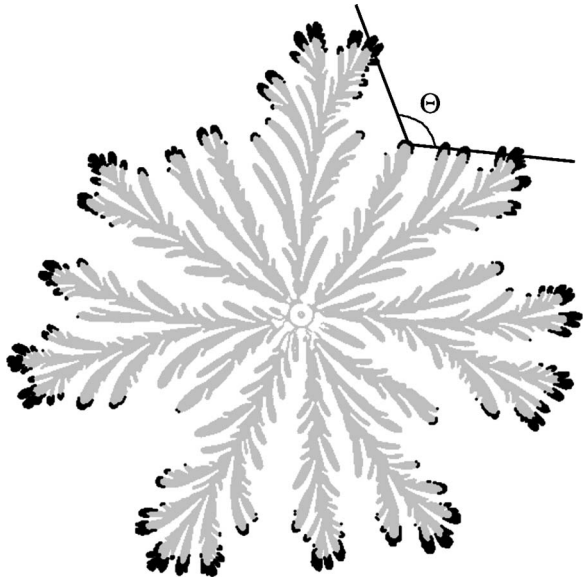

FIG. 10. Illustration of the definition of the unscreened angle Θ. Gray indicates structure that had grown to $r_{max}/b=660$ (ratio of pattern radius to gap thickness) at time=2.1 s ($\Delta P=1.25$ atm), and black shows the additional growth in the subsequent 0.17 s. The growth is concentrated at the tips of the branches. For every point on the boundary between the preexisting (gray) and active (black) regions, we define an unscreened angle Θ, which is the largest angle that can be drawn from the point without including any point of the preexisting pattern.

results in Fig. 8(b), which is reflected by the error bars in Fig. 9 for $q<0$, is essentially statistical.

The spectra of generalized dimensions D_q were also obtained for other values of ΔP, and we found that the range in which the pattern can be considered a fractal object decreases with decreasing ΔP. However, as Fig. 9 illustrates, the results obtained for D_q for different ΔP are the same within the experimental uncertainties. The apparent slight difference in the functional dependence of the D_q curves for $q>0$ and $q<0$ appears to be a difference in the results given by the two algorithms rather than a property of the fractal structure of the pattern; the difference is within the uncertainties (cf. Fig. 9).

Thus we conclude that D_q is independent of q for viscous fingering patterns in the limit of small gap and high forcing, i.e., the patterns are *self-similar*. Simulations of diffusion limited aggregation [20,21,35,40,41] have also yielded a monofractal (constant D_q) structure for DLA clusters. Hence the fractal morphology of viscous fingering patterns and DLA clusters is the same within the limits of experimental and numerical resolution. This *self-similar* property was also reported for two-dimensional electrodeposition clusters in the limit of small ionic concentration and high voltage [42]. Thus it appears to be a general property of asymptotic fractal structures grown in a Laplacian field.

V. UNSCREENED ANGLE

To characterize the growth process, we consider the screening effect that occurs during the growth. Growth along

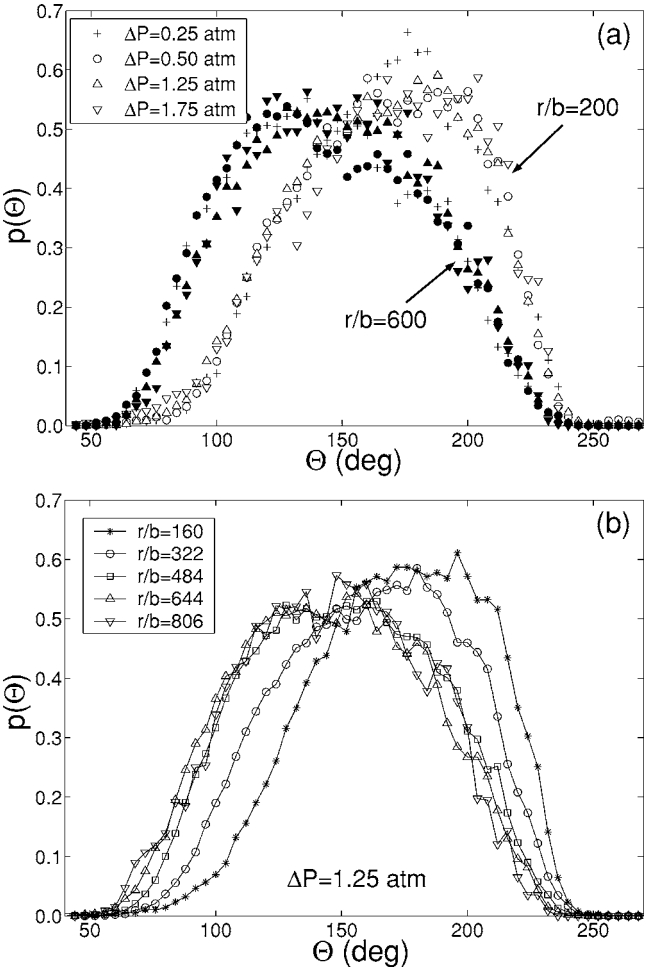

FIG. 11. Probability distribution of the unscreened angle. (a) The distribution function at each stage of the growth is independent of the forcing ΔP, as these two examples at different values of r/b illustrate. (b) The evolution of the probability distribution toward an asymptotic distribution is illustrated with these data for $\Delta P=1.25$ atm.

the boundary of the pattern is concentrated at the outer tips (where the pressure gradient is highest), as Fig. 10 illustrates. The probability of growth decreases toward the center of the cell. During the growth process, the active region moves outward, leaving behind "dead zones," which are shielded by the outer tips. This feature of Laplacian growth occurs also for DLA, where it is highly unlikely that a random walker will penetrate into the inner region.

We investigate the screening effect following a procedure used by Kaufman *et al.* [43], who determined the distribution of unscreened angles for growing DLA clusters. Images of the cluster at successive time steps reveal the "active region" where growth occurs. For each point on the boundary of the active region at an instant of time, we define the *unscreened angle* as the largest angle that can be drawn from this point without including any of the preexisting pattern (Fig. 10). Probability distributions for the unscreened angles obtained this way are found to be insensitive to the size of the time step used to identify the active region, provided that the time step is large enough so the boundary between the active and

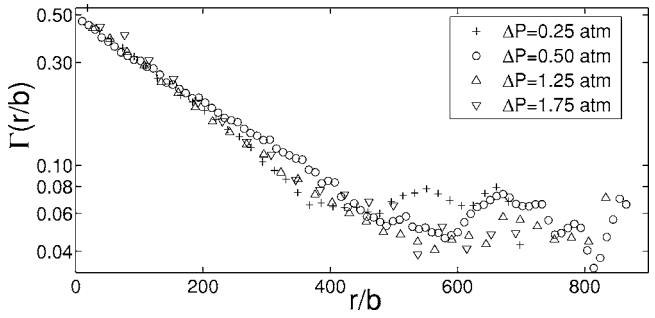

FIG. 12. Evolution of Γ, which is the root mean square departure of distribution function $p_r(\Theta)$ from the asymptotic distribution, $p_{asymp}(\Theta)$, as a function of the size of the pattern r/b [see Eq. (5)]. This semilog plot illustrates the exponential approach to the asymptotic distribution, $\Gamma \sim \exp[-(r/b)/\xi]$, where $\xi=200$. For $r/b > 500$, the distribution has reached the asymptotic distribution within our noise level.

preexisting regions remains unchanged even though the active region increases in size.

The probability distribution $p(\Theta)$ of the unscreened angle evolves during the growth of the pattern, but at any point in the growth, the distribution is the same at different ΔP, as Fig. 11(a) illustrates. This independence of forcing is consistent with our finding of an independence of the fractal dimension on ΔP.

In early stages of growth, the pattern does not exhibit much ramification. Most of the active regions have enough room to grow and are not strongly affected by the neighboring branches; the mean unscreened angle is large and the distribution function is negatively skewed [cf. Fig. 11(b) for $r/b=160$]. As the pattern continues to grow, the main branches develop more and more side branches, and these ramifications increase the screening effect. The mean of the probability distribution function for the unscreened angles, $p(\Theta)$, shifts toward smaller angles and becomes symmetric, converging to an invariant asymptotic form, $p_{asymp}(\Theta)$ [see Fig. 11(b) for $r/b=484$, 644, and 806]. This is the first report of the convergence. Such a measure of the screening effect has not been investigated previously for radial viscous fingering; also, for DLA clusters, the distribution function of unscreened angles reported by Kaufman *et al.* [25,43] was integrated in time.

To quantify the convergence of the distribution of the unscreened angle, we introduce the function

$$\Gamma(r) = \frac{1}{2\pi}\left[\int [p_r(\Theta) - p_{asymp}(\Theta)]^2 d\Theta\right]^{1/2}, \qquad (6)$$

which gives, at a given ΔP, a measure of the difference between the distribution $p_r(\Theta)$ (obtained for a pattern of radius r) and the final distribution, $p_{asymp}(\Theta)$. The evolution of Γ as a function of r/b is shown in Fig. 12. For all experimental conditions, $p_r(\Theta)$ converges exponentially fast toward $p_{asymp}(\Theta)$, and the e-folding length scale is $r/b=200$ (Fig. 12). The collapse of the different curves in Fig. 12 indicates that, at large forcing, the evolution of the distribution function is governed by r/b. For $r/b > 500$, the distribution has reached $p_{asymp}(\Theta)$ within our signal-to-noise level.

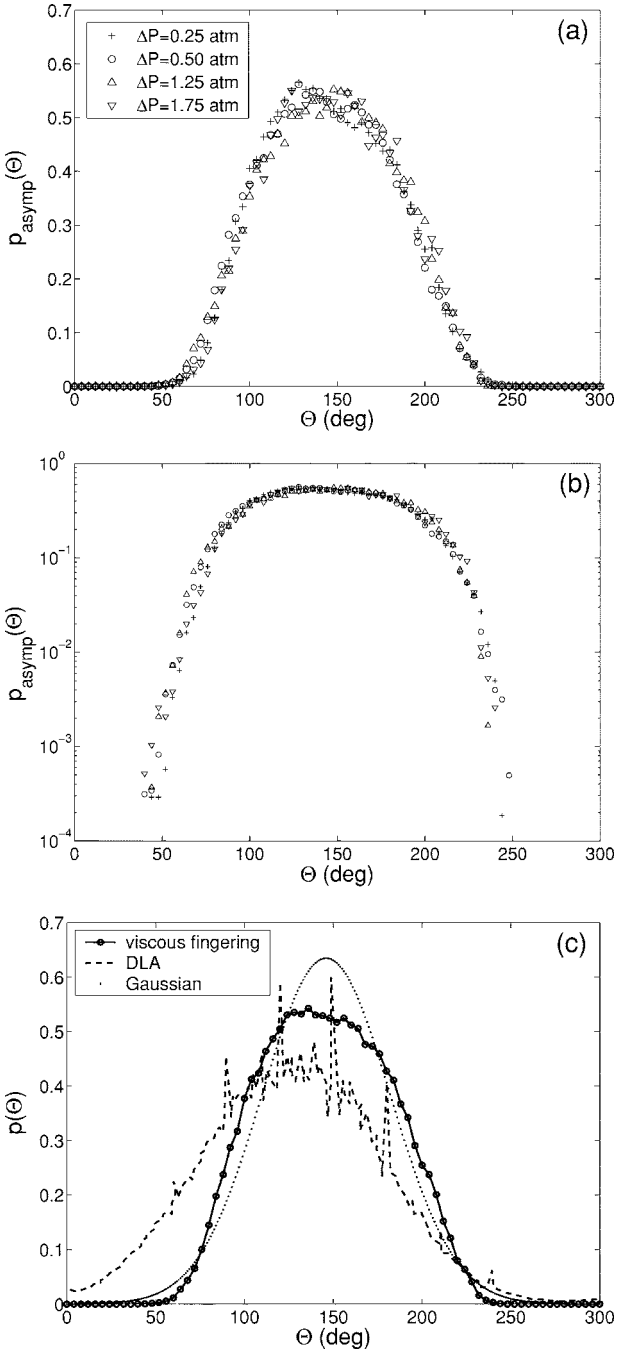

FIG. 13. Asymptotic probability distribution function for the unscreened angle: (a) linear plot, (b) semilog plot, (c) comparison of the average measured asymptotic distribution (solid line) with the distribution function calculated in an on-lattice DLA algorithm (dashed line) [25] and with a Gaussian distribution of the same mean and variance as the measured distribution (dotted line). Data in (a) and (b) for different forcings ΔP fall on a single curve, indicating the independence of the forcing. The data are for $r/b > 500$ [cf. Fig. 11(b)].

Our measurements of the asymptotic distribution of unscreened angles for four values of ΔP all superpose, indicating that $p_{asymp}(\Theta)$ is self-similar, as the linear and semilog

plots in Figs. 13(a) and 13(b) illustrate. The observed distribution is compared in Fig. 13(c) to one calculated using an on-lattice algorithm for DLA clusters [25,43].

For both large and small angles, the screening angle distribution decreases continuously (cf. Fig. 13) with no suggestion [within our resolution of 10^{-3} in $p(\Theta)$] of a cutoff where $p(\Theta)$ would be zero below a minimum angle. Similarly, there is no suggestion of a cutoff at a maximum angle. The properties of the measured asymptotic distribution and the on-lattice DLA distribution [25] are, respectively, mean angle 145°,127°; standard deviation 36°,51°; skewness 0.06,0.3; and kurtosis 2.3,3.8. The mean screening angle has also been computed for an off-lattice DLA algorithm, which yielded 151° [25], closer to our measured screening mean angle than obtained for on-lattice DLA.

VI. CONCLUSIONS

We have presented measurements of radial viscous fingering that have been shown to reach the asymptotic regime. To reach this asymptotic regime, both the forcing and the relative cluster radius r/b must be sufficiently large. In our experiments, the forcing parameter C (see Sec. III and Table I) reached about 800, and the ratio of the largest radius of the pattern to gap thickness r/b reached 900; both of these parameters are far larger than in previous experiments. We found the asymptotic state was achieved for $r/b=500$, which is less than half the cell radius ($r/b=1100$); hence boundary effects are negligible [cf. Fig. 2(a)].

The fractal dimension measured for the asymptotic viscous fingering patterns is $D_0=1.70\pm0.02$, where the uncertainty includes both the statistical uncertainty determined from multiple measurements and an estimate of systematic uncertainty in our box counting algorithm. Calculations of the generalized dimension D_q for positive and negative q have revealed no discernible q dependence for the ranges examined: for $-11\leqslant q\leqslant 0$, $D_q=1.70\pm0.1$ and for $0\leqslant q\leqslant 17$, $D_q=1.70\pm0.04$. Thus within the accuracy of our measurements, we conclude that radius viscous fingering patterns formed with high forcing are monofractals with $D_q=1.70$, independent of q.

We have found that the distribution function for the unscreened angles is independent of the strength of the forcing throughout the whole evolution of the patterns. In particular, the *asymptotic* distribution is independent of forcing; thus it provides a quantitative description of the screening effect.

The measured asymptotic distribution (Fig. 13) has a broad peak with a well-defined mean of 145°, which is close to the critical angle obtained in DLA simulations [22,23,25] and close to $2\pi/5=144°$, associated with fivefold symmetry [19–21,24]. However, we find no evidence of any macroscopic fivefold structure: the asymptotic distribution is broad with a standard deviation of 36°, and there is no obvious relation between the distribution function for unscreened angles and the existence of a critical angle or a pentagonal symmetry. Thus it may be a coincidence that the mean of the asymptotic distribution is close to $2\pi/5$.

In conclusion, our determination of an invariant asymptotic distribution of unscreened angles provides a new property that will help in the development of a theory of Laplacian growth of fractal patterns [17,44–46]. Our measured distribution function of unscreened angles is qualitatively (but not quantitatively) similar to that found in an on-lattice computation for DLA [25]; it would be interesting to compare the measurements with an off-lattice DLA computation.

ACKNOWLEDGMENTS

We thank James Kaufman, Mark Mineev, William D. McCormick, Mitchell Moore, Leonard Sander, Eran Sharon, and Matt Thrasher for helpful discussions. This work was supported by the Office of Naval Research.

[1] D. Bensimon, L. P. Kadanoff, S. D. Liang, B. I. Shraiman, and C. Tang, Rev. Mod. Phys. **58**, 977 (1986).
[2] P. Pelcé, *Dynamics of Curved Fronts* (Academic Press, San Diego, 1988).
[3] K. V. McCloud and J. V. Maher, Phys. Rep. **260**, 139 (1995).
[4] Y. Couder, in *Perspectives in Fluid Dynamics*, edited by G. K. Batchelor, H. K. Moffatt, and M. G. Worster (Cambridge University Press, Cambridge, 2002), pp. 53–104.
[5] R. L. Chuoke, P. van Meurs, and C. van der Poel, Trans. AIME **216**, 188 (1959).
[6] L. Paterson, Phys. Rev. Lett. **52**, 1621 (1984).
[7] T. A. Witten and L. M. Sander, Phys. Rev. Lett. **47**, 1400 (1981).
[8] L. M. Sander, P. Ramanlal, and E. Ben-Jacob, Phys. Rev. A **32**, 3160 (1985).
[9] F. Barra, B. Davidovitch, A. Levermann, and I. Procaccia, Phys. Rev. Lett. **87**, 134501 (2001).
[10] R. C. Ball and E. Somfai, Phys. Rev. Lett. **89**, 135503 (2002).
[11] F. Barra, B. Davidovitch, and I. Procaccia, Phys. Rev. E **65**, 046144 (2002).
[12] S. N. Rauseo, P. D. Barnes, and J. V. Maher, Phys. Rev. A **35**, 1245 (1987).
[13] Y. Couder, in *Random Fluctuations and Pattern Growth: Experiments and Models*, edited by H. E. Stanley and N. Ostrowsky, (Kluwer Academic Publishers, Dordrecht, 1988), pp. 75–81.
[14] S. E. May and J. V. Maher, Phys. Rev. A **40**, 1723 (1989).
[15] B. B. Mandelbrot and C. J. G. Evertsz, Nature (London) **348**, 143 (1990).
[16] T. C. Halsey, B. Duplantier, and K. Honda, Phys. Rev. Lett. **78**, 1719 (1997).
[17] M. H. Jensen, A. Levermann, J. Mathiesen, and I. Procaccia, Phys. Rev. E **65**, 046109 (2002).
[18] E. Lajeunesse and Y. Couder, J. Fluid Mech. **419**, 125 (2000).
[19] A. Arneodo, F. Argoul, J. F. Muzy, and M. Tabard, Phys. Lett. A **171**, 31 (1992).

[20] A. Arneodo, F. Argoul, J. F. Muzy, and M. Tabard, Physica A **188**, 217 (1992).
[21] A. Arneodo, F. Argoul, E. Bacry, J. F. Muzy, and M. Tabard, Phys. Rev. Lett. **68**, 3456 (1992).
[22] D. A. Kessler, Z. Olami, J. Oz, I. Procaccia, E. Somfai, and L. M. Sander, Phys. Rev. E **57**, 6913 (1998).
[23] G. M. Dimino and J. H. Kaufman, Phys. Rev. Lett. **62**, 2277 (1989).
[24] A. Kuhn, F. Argoul, J. F. Muzy, and A. Arneodo, Phys. Rev. Lett. **73**, 2998 (1994).
[25] J. H. Kaufman, G. M. Dimino, and P. Meakin, Physica A **157**, 656 (1989).
[26] E. Sharon, M. G. Moore, W. D. McCormick, and H. L. Swinney, Phys. Rev. Lett. **91**, 205504 (2003).
[27] L. M. Sander (private communication).
[28] P. Grassberger and I. Procaccia, Physica D **9**, 189 (1983).
[29] P. Grassberger and I. Procaccia, Phys. Rev. Lett. **50**, 346 (1983).
[30] P. Meakin, *Fractals, Scaling and Growth Far from Equilibrium* (Cambridge University Press, Cambridge, 1998).
[31] P. Grassberger, Phys. Lett. **97A**, 224 (1983).
[32] A. Arneodo, G. Grasseau, and E. J. Kostelich, Phys. Lett. A **124**, 426 (1987).
[33] E. Ben-Jacob, G. Deutscher, P. Garik, N. D. Goldenfeld, and Y. Lareah, Phys. Rev. Lett. **57**, 1903 (1986).
[34] S. Tolman and P. Meakin, Phys. Rev. A **40**, 428 (1989).
[35] P. Ossadnik, Physica A **176**, 454 (1991).
[36] B. Davidovitch, A. Levermann, and I. Procaccia, Phys. Rev. E **62**, R5919 (2000).
[37] A. Renyi, *Probability Theory* (North Holland, Amsterdam, 1970).
[38] P. Grassberger and I. Procaccia, Physica D **13**, 34 (1984).
[39] R. Badii and A. Politi, Phys. Rev. Lett. **52**, 1661 (1984).
[40] T. Vicsek, F. Family, and P. Meakin, Europhys. Lett. **12**, 217 (1990).
[41] W. G. Hanan and D. M. Heffernan, Chaos, Solitons Fractals **12**, 193 (2001).
[42] F. Argoul, A. Arneodo, G. Grasseau, and H. L. Swinney, Phys. Rev. Lett. **61**, 2558 (1988).
[43] J. H. Kaufman, O. R. Melroy, and G. M. Dimino, Phys. Rev. A **39**, 1420 (1989).
[44] T. C. Halsey, P. Meakin, and I. Procaccia, Phys. Rev. Lett. **56**, 854 (1986).
[45] R. C. Ball, Physica A **140**, 62 (1986).
[46] I. Procaccia and R. Zeitak, Phys. Rev. Lett. **60**, 2511 (1988).